Thermal effects in spin-torque assisted domain wall depinning

Björn Beyersdorff,* Sebastian Hankemeier, Stefan Rößler, Yuliya Stark, Germar Hoffmann,†
Robert Frömter, and Hans Peter Oepen
Institut für Angewandte Physik, Universität Hamburg, Jungiusstraße 11, 20355 Hamburg, Germany

Benjamin Krüger
I. Institut für Theoretische Physik, Universität Hamburg, Jungiusstraße 9, 20355 Hamburg, Germany
(Received 14 May 2012; published 26 November 2012)

We have investigated the magnetization reversal in V-shaped permalloy (Py) nanowires under high dc currents via anisotropic magnetoresistance (AMR) measurements. Utilizing a diamond substrate as heat sink, current densities up to 2×10^{12} A/m^2 can be applied. These high current densities enabled us to observe spin-torque assisted switching in thermal equilibrium, without the influence of transient effects. At high currents, the field driven magnetization reversal process is influenced by Joule heating, Oersted fields, and spin-torque effects. These contributions can be identified in our experiment due to their different symmetry properties under magnetization and current reversal. We obtain two important results when evaluating the spin-torque efficiency ϵ, which is proportional to the nonadiabaticity parameter β. First, we find different values for ϵ within the same sample, obtained with just a slight variation of the experimental parameters. Second, within the temperature range of 77 to 327 K, ϵ is found to be constant.

DOI: 10.1103/PhysRevB.86.184427 PACS number(s): 75.76.+j, 75.60.Jk, 75.60.Ch, 75.47.−m

I. INTRODUCTION

Utilizing spin-polarized electrons to manipulate the local magnetization is believed to lead to the development of novel devices[1] in the field of spintronics.[2] Spin-polarized currents interact with the magnetization in a way that can be understood as a torque. Adiabatic and nonadiabatic spin-transfer torques (STT) can result in a domain wall displacement.[3] To realize STT in devices, a fundamental understanding of the different torque terms is mandatory. The adiabatic torque, where the spins of the conduction electrons follow the local spatially varying magnetization, is well understood and is described in the framework of a number of different transport theories.[4–7] In contrast, the strength and origin of the non-adiabatic contribution is subject of present debate.[8,9] Various mechanisms are suggested to explain its origin, such as momentum transfer,[4,7] spin mistracking,[6,10] or spin-flip scattering.[11] In this context, it is predicted that large nonadiabatic effects should appear in narrow domain walls because of large magnetization gradients.[5] The contribution and the strength of the non-adiabatic term is expressed phenomenologically by the dimensionless parameter β within the modified Landau-Lifshitz-Gilbert equation.[11,12] Recent first-principles calculations suggest that β is of the same order of magnitude as the damping parameter α.[13] Experimentally, spin-transfer-torque effects have been studied using numerous different methods focusing on the beta parameter (for an overview, see references in Refs. 9 and 14). Nearly all investigations have in common that to avoid damage by Joule heating, short current pulses with pulse durations in the range of nano- to microseconds are used to study STT effects. It is found that such pulsed currents can be used to manipulate domain walls. These experiments, however, are not conducted in thermal equilibrium. More or less strong temperature transients are generated, which can modify the interaction, and the results may thus deviate from those obtained under equilibrium conditions. In addition, a possible inherent temperature dependence of β, as mentioned in Ref. 15, could be responsible for an increased scatter of data. Furthermore, it is well known and already applied in devices that the collective dynamics of a magnetization distribution, which can be influenced by the slope and duration of a current pulse, will strongly influence the depinning from a barrier.[16,17] It is reasonable to speculate that the experimental conditions determine the attainable values for β. As a matter of fact, published values of β vary more than two orders of magnitude from 0.01 to 4.07.[18–20] To minimize uncertainties due to time effects, we follow a different approach for the investigation of nonadiabatic STT effects. To investigate the influence of temperature on STT we utilize dc currents and probe the influence of the current on depinning processes via the anisotropic magnetoresistance. As a sample, we use a V-shaped permalloy (Py) nanowire that is prepared on a diamond single crystal. The diamond substrate is mounted on a LN_2 cryostat. As the thermal conductivity of the diamond is high the whole substrate acts as a very effective heat sink. The temperature rise due to Joule heating is moderate even if dc current densities up to 2×10^{12} A/m^2 are applied.[21] The temperature at the diamond interface that is attached to the cryostat is kept at 77 K. An external magnetic field is used to generate or annihilate domain walls in the Py wire. The critical fields for nucleation and annihilation of the domain walls are investigated as a function of temperature and current density.

II. EXPERIMENTAL

The scanning electron micrograph in Fig. 1(a) shows the wire and the contact pads which are the bright areas on the right-hand and left-hand sides. A sketch of the wire geometry is displayed in Fig. 1(b). The permalloy wire was deposited via electron beam evaporation through a Si_3N_4 shadow mask and has a thickness of 18 nm.[21] The contact pads are Pt (10 nm)/Cr (10 nm) bilayers. The wire between the contact pads has a length of 20 μm. The angle between the two

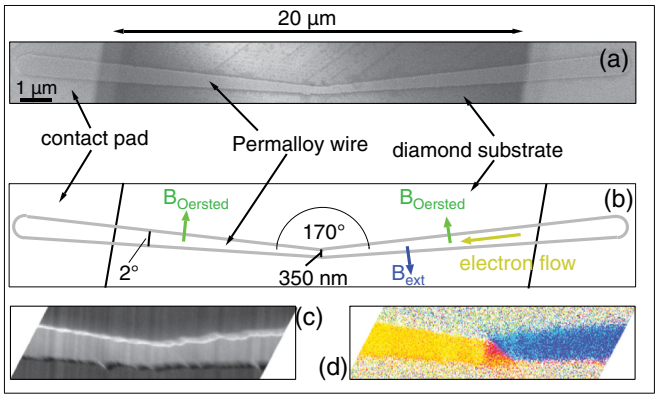

FIG. 1. (Color online) Experimental geometry. (a) SEM micrograph of the V-shaped wire used for the measurements. (b) Sketch of the experimental geometry. The blue arrow indicates the direction of the external magnetic field. The Oersted field (green arrows) is caused by a vertically nonuniform current distribution (green arrows). The corresponding current direction is given in yellow. This direction of the electron flow is taken as negative in the paper. (c) Zoom into the bend region. (d) Domain structure at the kink of the wire measured with SEMPA. Color wheel according to Fig. 3(c).

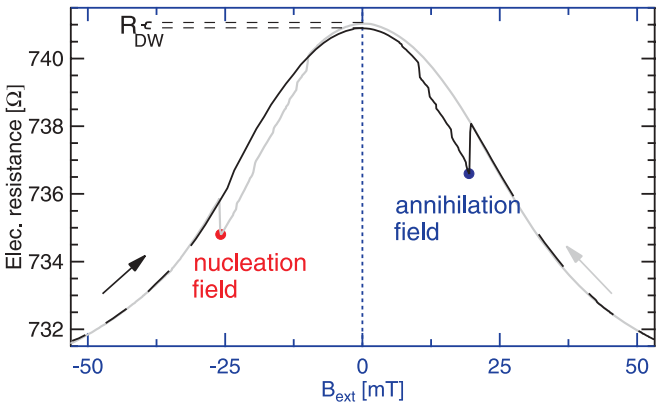

FIG. 2. (Color online) Resistance vs field curve obtained for the wire shown in Fig. 1 ($T_{\text{sample}} = 77$ K). The black and gray arrows indicate the directions of the field sweep. Blue and red circles mark jumps in resistance, which correspond to irreversible magnetic switching of the arm on the left-hand side. The difference in resistance at 0 mT between up and down sweep ($R_{\text{DW}} = 0.2\,\Omega$) is caused by the presence of a domain wall at the kink during the up sweep [see Fig. 1(d)].

arms of the V-shaped wire is 170°. The arms are trapezoidal with an opening angle of 2°, which gives the highest current density within the bend region where the wire has a smallest width of $w = 350$ nm. The peak-to-peak edge roughness is below 30 nm [see Fig. 1(c)]. We probe the magnetic state of the V-shaped wire via the anisotropic magnetoresistance (AMR). The magnetic field B_{ext} is applied in the film plane along the direction given by the blue arrow in Fig. 1(b). In the right arm, the magnetic field is perpendicular to the wire, so a reversal of the magnetization orientation cannot occur within the available fields. However, the field can cause irreversible switching of the left arm. The incoherent switching shows up as a jump in the resistance measurement. The corresponding field values are denoted as critical field B_{crit}.

III. RESULTS

A. Field loop

The magnetoresistance (MR) of a single field loop is plotted in Fig. 2 for a current density of 1.5×10^9 A/m^2. The overall shape of the curve exhibits a $\cos^2$ dependence, which is the signature of the AMR[22] when the magnetization is gradually rotated out of the direction of the current. Superimposed on this overall behavior we find discontinuities in the MR loops. These jumps are caused by abrupt changes of the micromagnetic structure of the V-shaped wire. Micromagnetic simulations have been performed by means of the object oriented micromagnetic framework (OOMMF)[23] to understand the details of the AMR curve and to correlate changes of the micromagnetic structure with discontinuities of the resistance. Based on the microstructure obtained from simulations [see Fig. 3(c)], AMR curves are calculated as shown in Fig. 3(b). As the magnetic field is oriented perpendicular to the arm on the right-hand side it causes a unison rotation of magnetization but not a change of the single-domain state. For that reason, a single-domain state is assumed on the right-hand side in the simulations. The AMR has been calculated only within the region indicated by the vertical dashed lines in Fig. 2(c). On the left-hand side, the wire is prepared on top of the contact pad for about 5 μm, the latter acting as current shunt. The contribution to the AMR from this region is thus strongly reduced and can be neglected in the AMR calculation.

The MR curve obtained from the simulations [see Fig. 3(b)] is very similar to the experimental one [see Fig. 3(a)]. Without field the magnetization is aligned parallel to the arms of the wire in a tail-to-tail domain configuration. A transverse domain wall is located at the constriction in agreement with the

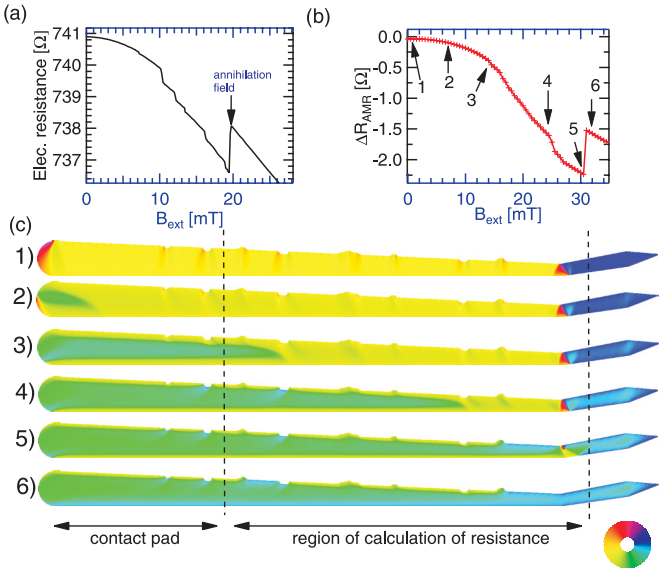

FIG. 3. (Color online) Micromagnetic structure (simulated via OOMMF) as function of field and the resulting field dependent AMR. (a) A zoom into the MR curve of Fig. 2 for increasing field. (b) The calculated AMR vs field curve that is estimated based on the simulated micromagnetic structure [panel (c)].

experimental result obtained via scanning electron microscopy with polarization analysis (SEMPA or spin-SEM[24]) [see Fig. 1(d)]. The magnetic "edge defect" is pinned at the inner edge of the kink of the V-shaped wire, as expected from topological considerations[25,26] [see Fig. 3(c)]. In the plot of the MR results, this domain pattern corresponds to the MR value where the black curve crosses the ordinate. On increase of the magnetic field, the magnetization starts to tilt out of the easy axis towards the field axis. This causes the observed decrease of the resistance. Comparing the micromagnetic structure at smallest fields, i.e., 0 mT [see "1" in Fig. 3(c)], 7 mT ("2"), and 14 mT ("3") it becomes obvious that a domain "wedge" nucleates at the end of the arm on the left-hand side and starts moving towards the kink. As soon as this wedge leaves the contact pad ("3"), the resistance shows a slight deviation from the parabolic behavior [see Fig. 3(b)]. This effect can also be seen in the measured MR curve. On further field increase negative jumps in resistance appear, which can be attributed to temporary pinning of the wedge followed by sudden release. The wedge moves to the next position of a local energy minimum or even to the equilibrium position as seen in the simulation ("4"). When arriving at the kink, the domain wedge eventually annihilates with the domain wall yielding a sudden resistance increase ("5" and "6"). This is the point where the domain wall vanishes (blue dot in Fig. 2). The height of the jump is a measure for the final position of the wedge in the wire. If the domain wall is depinned before the wedge has reached the kink, it causes an earlier reversal of magnetization and thus the observed jump is smaller.

When the field is reduced starting from the reversed state (grey line Fig. 2), the AMR signature of a continuous rotation remains. No jumps in resistance occur down to 0 mT. The corresponding domain structure in remanence is a single-domain state with magnetization pointing to the right. As this state is different from the starting domain pattern a different resistance is obtained (Fig. 2). The difference of 0.2 Ω must be attributed to the AMR signal of the domain wall, in accordance with results of Ref. 27. Increasing the field towards negative values reveals a similar scenario with the same signatures in the MR curve. As inversion to the former process, a domain wall is seeded at a certain value of the magnetic field. After cycling back to zero, the initial resistance value is obtained indicating that the seeded domain wall is still in the wire and is again a transverse domain wall. The MR measurements show different switching fields for wall annihilation ($+20$ mT) and creation (-25 mT).

At first sight, the existence of a transverse domain wall in remanence is surprising. The phase diagram for a similar geometry of the wire[28] suggests that a vortex wall is energetically more favorable. However, our simulations reveal that the appearance of a transverse wall is due to the orientation of the external field. While the external field is reduced towards zero, the magnetic moments inside the bend region are oriented almost like in a transverse wall. At vanishing fields the system relaxes into the local minimum of a transverse wall in remanence. The spin-SEM investigation confirms the existence of the transverse wall [see Fig. 1(d)]. In the following, we use the switching fields, indicated by blue (annihilation) and red symbols (creation) in the graphs, to investigate the annihilation and creation of the domain wall as a function of different parameters.

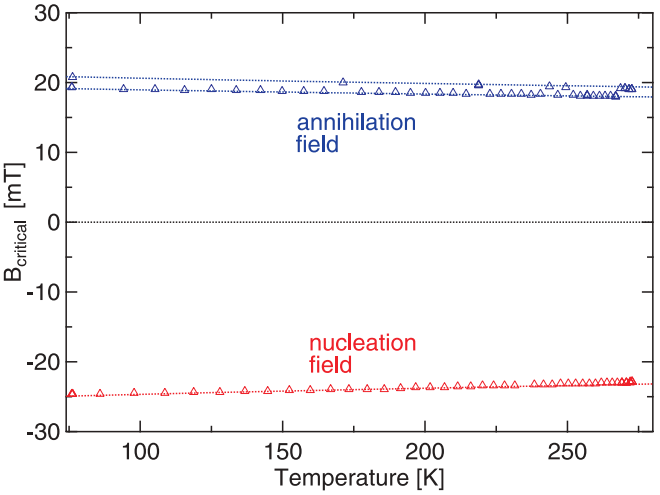

FIG. 4. (Color online) Switching fields as a function of temperature at lowest current density. The irreversible jumps that appear in the AMR loops (Fig. 2) are plotted as a function of temperature. The color coding is as indicated in Fig. 2.

B. Temperature variation

The dependence of the switching fields on substrate/wire temperature in thermal equilibrium is measured by varying the temperature of the cryostat (see Fig. 4). Each vertical slice through the graph represents a single MR loop similar to the loop in Fig. 2 at the particular temperature. Red triangles mark the nucleation, blue triangles the annihilation of the domain wall, respectively. The general trend is a decrease of the switching field with increased temperatures in accordance to previous findings.[29–31] The plot reveals that apparently two different pinning sites are effective for domain wall annihilation, as the blue dots in Fig. 4 accumulate stochastically around two discrete levels. The same feature is also visible in Fig. 5 where the effect of a variation of the current density is investigated. The reason for the existence of two pinning sites is the edge roughness of the wire in the region around the kink, visible in Fig. 1(c), which causes two slightly different annihilation characteristics, depending on the exact micromagnetic path the system takes.

C. Variation of current density

Next, the influence of an increasing current density has been studied. Figure 5(a) shows the nucleation and annihilation fields versus applied current density. The data have been obtained from single MR loops similar to the loop shown in Fig. 2. Three eye-catching features are visible in the graph: (I) a parabolic dependence of the annihilation field on current density (blue dots), (II) a linear slope of the nucleation field (red dots), and (III) an abrupt decrease of the annihilation field (blue dots) at high positive (see definition in Fig. 1) current densities. The data of Fig. 5(b) have been acquired by exactly the same measurement procedure as Fig. 5(a) but starting from a configuration with reversed magnetization orientation of the fixed arm (configuration "B"). Due to the reversed

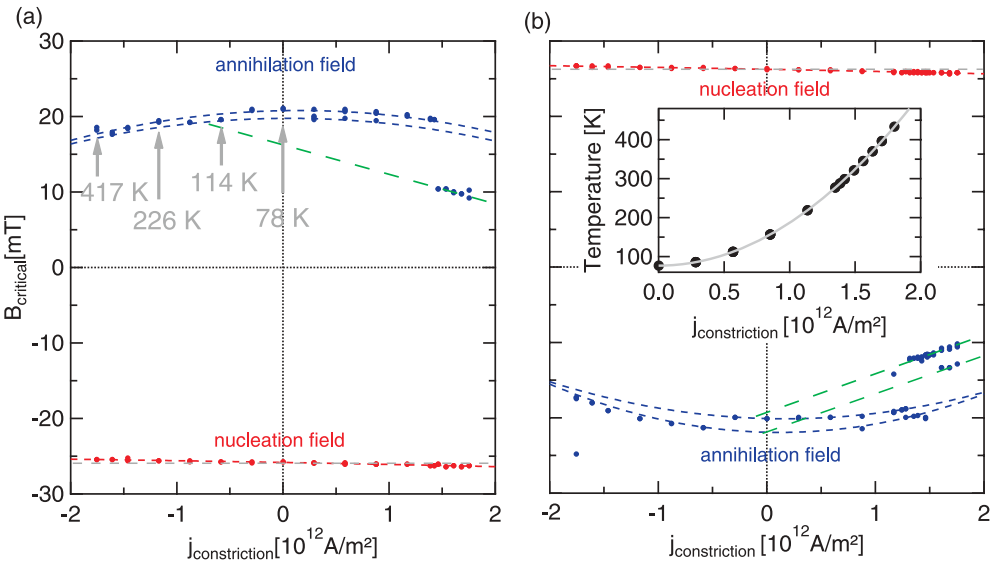

FIG. 5. (Color online) Switching fields as a function of current density. In Fig. 5(a) the result for the magnetic configuration shown in Figs. 1 and 2 is plotted, which is referred to as configuration "A" throughout the text. (b) Displays the result of the configuration "B" where the magnetization of the arm on the right-hand side is reversed while the same measurement routine is applied. The inset in Fig. 5(b) displays the temperature increase at the kink due to Joule heating. The gray line is a parabolic fit to the data (black dots).

magnetization orientation, the domain wall is now nucleated at positive and annihilated at negative fields. In the following, the different features of the graph are discussed and possible mechanisms proposed.

The parabolic dependence of the annihilation fields on current density reflects Joule heating of the wire. The reason for the parabolic behavior is that the temperature at the constriction is proportional to the applied heating power $P = R(T) \times I^2 \propto T_{\text{constriction}}$. The temperature in the constriction can be calibrated from the temperature dependence of the switching field (see Fig. 4) that allows to appoint the switching fields (blue dot) at given current density to a constriction temperature [indicated as gray numbers in Fig. 5(a); extrapolating from the data of Fig. 4 for temperatures above 300 K]. A plot of temperature versus current density is given as inset in Fig. 5(b). The gray line in the inset represents a parabolic fit to the data that demonstrates that the supposed correlation of temperature and current is correct. The temperature values agree fairly well with former results of measuring the average temperature increase of a straight wire on a diamond substrate.[21] In the latter experiments, the temperature was determined via the change of electrical resistance, i.e., via the $R(T)$ dependence. In contrast, the temperature in Fig. 5 was determined via temperature-dependent magnetic switching; both approaches give the same result.

Next, we discuss the nucleation fields (red dots in Fig. 5). The nucleation fields show a weak linear dependence on variation of current density. The red dashed line is a linear fit to the data points and demonstrates the weak dependence on current density. For comparison, the grey dashed line represents a hypothetical case of constant switching field. Both nucleation fields for the different starting configurations have the same slope with the same sign. Thus, in the case of positive currents, the switching is hindered for negative field values and supported for positive ones. For negative currents, the nucleation fields are affected in the reversed manner. This symmetric behavior under current and magnetization (i.e., field) reversal is characteristic for Oersted field effects.[32–34] In Fig. 1(b), the Oersted field and its orientation with respect to the external field is shown for the situation mentioned above. A possible explanation for the existence of an Oersted field can be found in Ref. 34.

The third and most interesting feature is the abrupt decrease of the switching field at a positive current density of 1.2×10^{12} A/m^2. Towards higher current densities the drop is followed by a linear decline of the switching field. It is marked by green dashed lines that are meant as a guide to the eye. This feature is only visible for positive current densities (for definition see Fig. 1). It reveals the same symmetry for both magnetization configurations yielding a decrease in switching field with increasing current. Thus it cannot be caused by an Oersted field. Instead, the very similar behavior under magnetization reversal can be explained by spin torque. It originates from the fact that the spin torque acts in the same way on head-to-head and tail-to-tail walls: it pushes the wall into the direction of the electron flow. The abrupt decrease in switching field is the spin-torque-assisted depinning of a domain wall.[36] For current densities below 1.2×10^{12} A/m^2, an influence of the current is not observed. The linear extrapolation of the spin-torque assisted switching fields towards zero current yields two slightly different field values that may be caused by different pinning sites of the wall.

To increase the effective field along the wire axis, the field was further tilted towards the wire axis in a subsequent experiment. For a field applied at an angle of 7° with respect to the bisecting line (which is only differing by 2° from the previous measurement), the results are displayed in Fig. 6. At this angle both arms of the wire become switchable. The maximum field, however, that was applied during the

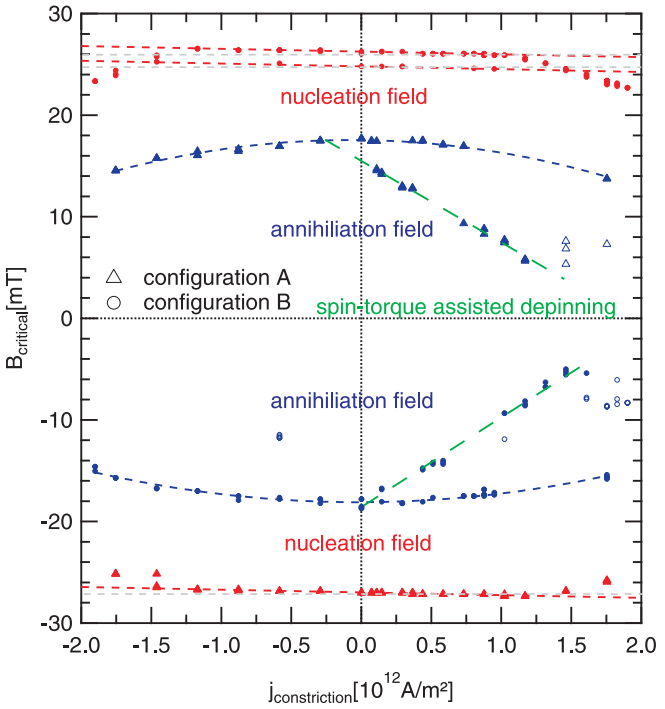

FIG. 6. (Color online) Switching field as a function of current density for a different field orientation. The field is tilted 7° to the bisecting line of the two arms (i.e., 2° more than in Fig. 5). Configurations "A"/"B" are given by triangles and circles, respectively. The spin-torque signature can be observed for almost all positive current densities. It reduces the critical field. Data points not lying on the dashed linear slope are marked with open symbols.

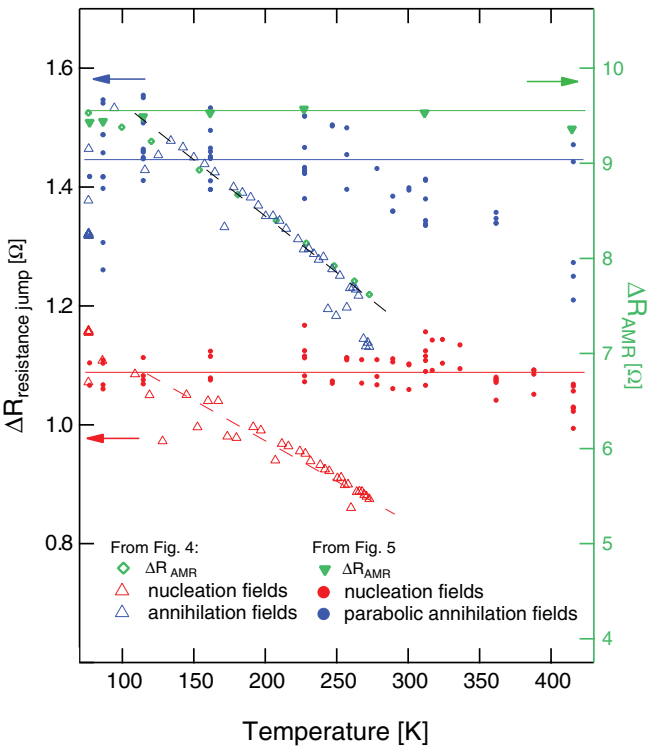

FIG. 7. (Color online) Height of the resistance jumps (blue/red symbols, left ordinate) and overall AMR signal [$\Delta R_{\mathrm{AMR}} = R\,(0\,\mathrm{mT}) - R\,(54\,\mathrm{mT})$, green symbols, right ordinate] vs temperature. The data from Fig. 4 (open symbols) are measured with the whole system in thermal equilibrium. The relative change versus temperature is almost the same for all three signals (AMR: green diamonds, annihilation: blue triangles, nucleation: red triangles). For comparison, the same signals (AMR, annihilation, nucleation) are plotted in the case when a current is driven through the wire (taken from Fig. 5, full symbols) which causes Joule heating. The temperature in the latter case is a local temperature at the kink where the domain wall is located before release. The almost constant signal height indicates that the MR signal is generated at a location where the temperature is not strongly changing, i.e., in the arm of the wire on the left-hand side. Lines are meant as guide to the eye.

sweeps has been reduced to a value that no irreversible changes of the magnetic microstructure occur in the part of the wire on the right-hand side (neither with nor without applied current). In this geometry, we observe a reduction of the critical field at vanishing current density from 20 to 18 mT. This change can be attributed (within the error margin of 1°) to the dependence of the switching field[35] on the external field orientation. Hence the magnetic processes determining the switching should be similar to the ones in the previous investigation (see Fig. 5). In Fig. 6, data for both starting configurations are combined in one graph. Triangles/circles indicate the magnetic configurations "A" and "B" corresponding to the measurement of Figs. 5(a) and 5(b), respectively. The main features discussed in connection with Fig. 5 can be found in this measurement as well. A slight change is found in the nucleation processes. In configuration "A" a second, new nucleation site shows up. The Oersted-field contribution determined from Fig. 5 is given as straight lines through the data sets of both configurations (see Fig. 6). At high currents, some influence of Joule heating is now observable. The temperature effect appears to be stronger in configuration "A" for both nucleation sites. The temperature effects act in addition to or change the Oersted field contribution. The most notable difference, however, is the fact that no threshold for the current induced depinning process appears anymore. Both switching processes, the current-driven and the field-driven, seem to coexist. In Fig. 6, the annihilation fields for the spin-torque assisted switching show a linear dependence over almost the whole positive current-density range. Deviations from this linear behavior can only be found at very high current densities above 1.5×10^{12} A/m^2. For current densities above this value an increase in annihilation field appears. This might be due to the current induced formation of multivortex walls that have a higher critical current density.[37] Interestingly, the extrapolation of the linear dependence to zero current density gives different critical field values for the two configurations in both experiments (see Figs. 5 and 6). While in configuration "B" the critical field at zero current density is the same as for the field driven reversal, the value in configuration "A" is smaller, indicating two slightly different microstructures of the current-susceptible configuration in these cases.

To clarify whether the observed decrease of reversal field can be unambiguously attributed to spin torque the jump heights of the resistance at critical field are examined. First, we use the temperature calibration at the kink region (see inset in Fig. 5) to compare the jump heights for the different processes (see Fig. 7) and examine their temperature dependence. From

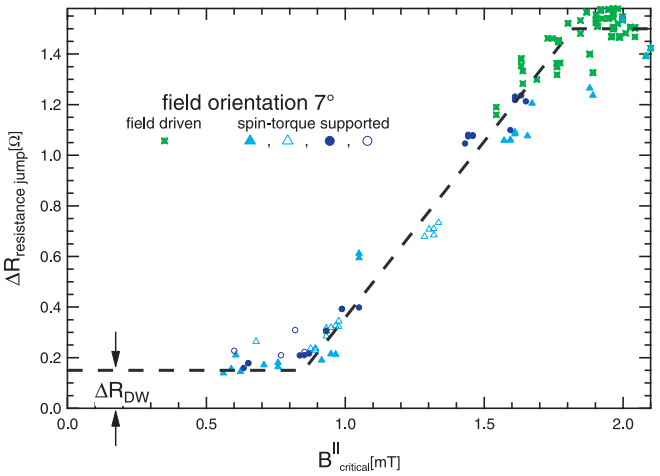

FIG. 8. (Color online) Height of resistance jumps (annihilation) as function of critical field. The projection of the switching field onto an imginated straight wire perpendicular to the bisecting line of the two arms (in plane) is used as abscissa. For low fields the height of the resistance jumps is constant and comparable to the domain wall resistance (see also Fig. 2). As with increasing field the domain wedge leaves the contact pad the resistance jump increases. These switching fields can be attributed to spin-torque-assisted depinning (data points of configuration A/B in light/dark blue, open/closed symbols as in Fig. 6). Green crosses represent resistance jumps due to the pure field-driven annihilation (blue parabolas in Fig. 6).

the experiments in thermal equilibrium (see Fig. 4), we can extract the resistance jumps for nucleation and annihilation (open triangles) as well as the total resistance change in maximum field (green open diamonds). From the latter plot, we obtain the temperature dependence of the AMR signal, which is in good accordance with literature.[22] Although the absolute numbers are different (different scaling of ordinates), the relative change of resistance versus temperature is almost identical for the total AMR and the annihilation/nucleation processes. The temperature dependence of the latter can therefore be solely attributed to the temperature dependence of the AMR. Comparing these graphs with the data (solid red and blue symbols) of the current-assisted switching (full circles), a completely different general trend is obtained. For current-assisted switching, the signals stay almost constant up to 250 K and decrease only slightly towards higher temperatures. At first sight, one might take this as an indication of a wrong temperature scaling for the current-assisted switching studies. On second thought, however, it comes to mind that the measured temperature distribution in the current-assisted experiments has to be considered. The temperature given in the inset of Fig. 5(b) is that of the kink. The signals, however, reveal almost no or a strongly reduced influence of temperature. This means that the temperature in the region where the MR signal originates from is considerably lower than at the kink. Vice versa, the temperature plot can be seen as a rough estimate for the position where the annihilation takes place. No significant temperature influence is observed up to a temperature of 300 K. which, using the temperature calibration at the kink (see Fig. 5 inset), corresponds to a current density of $\approx 1.4 \times 10^{12}$ A/m^2.

Next, the dependence of jump height on critical field is analyzed (see Fig. 8) in order to identify the location of the wedge front during annihilation. Only the jump heights of the annihilation fields are considered, as the nucleation fields are not affected by spin torque and do not show a strong dependence on critical field. In Fig. 8, the aforementioned resistance jump heights are plotted versus critical field for the experiment at a field orientation of 7°. Exactly speaking, the projection of the field perpendicular to the bisecting line of the angle between both arms has been taken as abscissa. The temperature dependence of the AMR signal is almost negligible for all spin-torque assisted switching events given by full blue symbols. For low critical fields, the height of the resistance jump is small and almost constant. This resistance change is almost the same as the value that is found for the transverse wall at zero field in the hysteresis loop given in Fig. 2. For small fields, the domain wedge is still in the region of the contact pads where the MR measurement has a vanishing sensitivity. As the rotation of the magnetization in the wire is also very small in low fields, it is solely the domain wall that rushes through the wire and causes the resistance change. This proves that the observed jumps in resistance at low field values are correlated to the depinning of the domain wall. As soon as the wedge extends beyond the contact pads, it starts to contribute to the measured magnetoresistance and the jump of resistance increases. The magnetic microstructure of the wedge causes a decrease of resistance as it contains parts where the magnetization is rotated out of the direction of the current. With increasing effective area of the domain wedge the resistance change becomes more pronounced. This interpretation is completely consistent with the observed temperature behavior of the jump heights. While the main AMR signal comes from the change of the microstructure of the wedge, which is in the cold part of the wire, the critical field, however, is the depinning field that is effective at the position of the wall, i.e., at the kink. The linear increase of the jump heights reflects the change of the domain structure on field increase. The jump height reaches a plateau at about 1.75 mT. This value is identical to the average jump height in field driven reversal. At the maximum value the domain wedge reaches almost the kink and either the field causes the reversal (at higher critical fields) or depinning is still effective.

In Fig. 9, the absolute value of the critical field versus current density is plotted for both measurements (see Figs. 5 and 7). B_{critical} is again the projection as defined above (see Fig. 8). Here it becomes obvious that all different jump values belong to the same mechanism as they apparently fit to one straight line for the respective configuration. Only a few data points (open symbols) that exhibit maximum jump heights (clustering in Figs. 5 and 7) do not fit to the line. As speculated above they obviously belong to a different annihilation process. They cluster around values that are comparable to the results of the low-angle experiment. In such a plot, the slope of the curve corresponds to the spin-torque efficiency ϵ.[39] A linear dependence of critical field on current density is evident at least for the experiment at the larger angle (blue symbols) for both configurations. As the temperature at the kink, where the domain wall is located, varies with current it is possible to introduce a temperature scale (upper ordinate). Even though our experiment does not directly separate current and temperature variation effects, we can show by a simple symmetry argument (see Appendix) that, as long as a linear

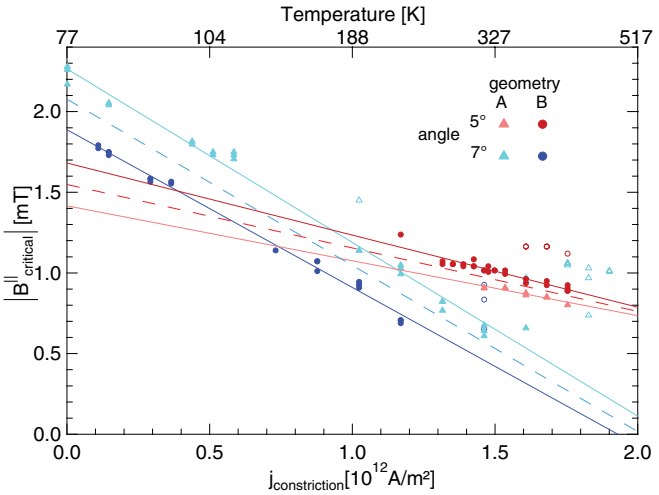

FIG. 9. (Color online) The projected critical field versus current density. The results for configuration "A"/"B" are given as triangles/circles, respectively. The filled symbols belong to the data points that fit to the lines given in the plots of critical field vs current density. Open symbols correspond to the data points that cluster at high current. The blue symbols are the results obtained in the field that is stronger tilted. The lines are least square fits to the data points with different geometries and configurations. The dashed lines give the fit to all data points of the same angle. The dark/light blue lines yield spin-torque efficiencies of $\epsilon = (1.07 \pm 0.02) \times 10^{-15}$ Tm^{2}A^{-1} and $(0.98 \pm 0.02) \times 10^{-15}$ Tm^{2}A^{-1}, respectively. The light/dark red symbols correspond to the experiment with smaller angle of field orientation and yield $\epsilon = (0.34 \pm 0.04) \times 10^{-15}$ Tm^{2}A^{-1} and $(0.45 \pm 0.03) \times 10^{-15}$ Tm^{2}A^{-1}. The averaged values that are obtained for configuration "A"/"B" are $\epsilon = (0.4 \pm 0.04) \times 10^{-15}$ Tm^{2}A^{-1} for 5° and $\epsilon = (1.03 \pm 0.02) \times 10^{-15}$ Tm^{2}A^{-1} for 7°, respectively.

dependency of critical field on current density is found, its slope is identical to the spin-torque efficiency that would be measured at fixed temperature. The Appendix demonstrates that with a parabolic dependence of temperature on current only a constant or even powers of ϵ with current are compliant. Careful data analysis leads to the conclusion that no significant higher-order terms in j are present. Hence the experiment proves that ϵ is not dependent on temperature. At least this is true for the temperature range covered in the second experiment (at 7° field orientation, blue symbols), i.e., from 77 to 327 K (see Fig. 7). Both fits in Fig. 9 indicate that for the experimental configuration Oersted fields do not influence the spin-torque efficiency, as in case of Oersted contributions the two lines for the two configurations should exhibit an increase of splitting with growing current density. The linear fits for the two configurations (at 7° field orientation) give spin-torque efficiencies of $\epsilon = (1.07 \pm 0.02) \times 10^{-15}$ Tm^{2}A^{-1} and $(0.98 \pm 0.02) \times 10^{-15}$ Tm^{2}A^{-1}. The average value (dashed line in Fig. 9) gives $\epsilon = (1.03 \pm 0.02) \times 10^{-15}$ Tm^{2}A^{-1}. Apparently, the average value of ϵ for the first experiment (red dashed line) yields a different slope of $\epsilon = 0.4 \times 10^{-15}$ Tm^{2}A^{-1}. The red full symbols correspond to current values beyond 1.4×10^{12} Am^{-1} and thus correspond to processes where the magnetic microstructure of the domain wedge comes close to the kink and thus can influence the fine structure of the domain wall. The latter can be responsible for affecting the depinning process.

The results imply that the spin-torque efficiency ϵ can vary for the same sample and details of the magnetic microstructure and the experimental geometry have to be taken into consideration in the interpretation. This sensitivity on the exact geometry and thus microstructure probably contributes a large amount to the scatter in different results obtained for the nonadiabaticity β (which is deduced from ϵ) in various publications.[18,20,39–41] Independent of the exact value of ϵ, which obviously varies for different geometries, our experiment shows that for a fixed geometry ϵ is temperature independent for actual wire temperatures from liquid nitrogen up to ambient conditions. This finding appears to be at variance to results published earlier,[38] where a 25 % increase of critical current density was found in the narrow temperature range from 100 to 170 K and a decrease of spin-torque efficiency was suggested as explanation. However, this is not the only possible interpretation, as a direct temperature dependence of the pinning potential can be supposed instead.[42] Following the model of Ref. 43, our findings on ϵ can be extended to discuss the effectiveness of adiabatic versus nonadiabatic spin torque in the depinning process. Within the regime of weak pinning and for a measurement that is performed in a constant current mode (not pulsed), the model predicts that depinning is governed by the nonadiabatic spin torque only and that the adiabatic contribution can be neglected. Thus conclusions on the nonadiabaticity parameter β can be inferred from our finding. According to Ref. 43 the spin-torque efficiency is proportional to $\beta P/M_S$. Thus it follows from our result, i.e., ϵ is constant in the temperature range investigated, that the temperature dependence of β is given by the variation of P/M_S with temperature. We have not measured this quantity so that we cannot give any hard numbers for the temperature dependence of β. Recently, the temperature dependence of the P over M_S ratio was measured for Py films of similar thickness.[44] The authors find only a moderate and more or less continuous decline of this ratio by 14% over the observed temperature range of 80 to 340 K. Using this number, it follows from our investigations that the β parameter itself should be only weakly depending on temperature. To be more precise, this would imply a continuous increase of β by 16% over the temperature range of our experiment. However, this is not a result that relies solely on the investigation presented in this paper.

IV. SUMMARY

In summary, it has been demonstrated that the effects of Joule heating, a transverse Oersted field, and spin-transfer torque on the switching of a two-domain state in a nanowire can be unambiguously separated. All three mechanisms generate different signatures in a plot of switching field versus current density. The influence of the Oersted field is found to be small compared to the spin-transfer-torque effect and both can be easily distinguished via their different symmetry properties regarding magnetization and current reversal. Within the error margin, the spin-transfer-torque efficiency does not show any temperature dependence between 77 and 327 K.

ACKNOWLEDGMENTS

Financial support by the Deutsche Forschungsgemeinschaft via the Sonderforschungsbereich 668 and the Forschungs und Wissenschaftsstiftung Hamburg via the Landesexzellenzcluster Nano-Spintronics is gratefully acknowledged. H. P. Oepen is grateful for hospitality at CIC nanoGUNE during his research stay. He is thankful to Basque foundation of Science for the financial support via an Ikerbasque visiting fellowship.

APPENDIX

It has been shown in Ref. 17 that the equation of motion of a transverse and a vortex domain wall can be written as

$$\ddot{X} = -\frac{\dot{X}}{\tau_d} - \frac{1}{m'}\frac{dE}{dX} + \frac{C_1}{\tau_d}H + C_2\dot{H} + \frac{C_3}{\tau_d}j + C_4\dot{j}. \quad \text{(A1)}$$

Here, τ_d and m' are the damping time and the mass of the wall, respectively. The effective prefactors C_1, C_2, C_3, and C_4 depend on the geometry of the wall. Equation (A1) is a linear response of the domain wall to the magnetic field H along the wire, the current density j in the wire, and their time derivatives. In the present experiment, the magnetic field and the current density change very slowly so that we can assume that $\dot{H} = 0$ and $\dot{j} = 0$. The condition for a depinning of the wall is a nonvanishing velocity at the position with the maximum restoring force. With

$$C_0 = -\frac{\tau_d}{m'}\max\left(\frac{dE}{dX}\right), \quad \text{(A2)}$$

one gets

$$0 = C_0 + C_1 H_d + C_3 j_d \quad \text{(A3)}$$

for the field H_d and the current j_d at which the domain wall depins. This equation is valid for a vanishing temperature. To take the temperature into account, we introduce a temperature dependence of the prefactors. This yields

$$0 = C_0(T) + C_1(T)H_d + C_3(T)j_d. \quad \text{(A4)}$$

The temperature is given by the cryostat temperature T_0 and the current density j in the sample due to the Joule heating. One finds (see inset in Fig. 5)

$$T = T_0 + a j_d^2, \quad \text{(A5)}$$

where a is given by the thermal conductivity of the substrate, the resistivity of the sample, and the geometry. From Eq. (A5), one can see that T is an even function in j_d. In principle, a may depend on T. However, such a dependence would not affect the conclusion that T is even in j_d and will be neglected for simplicity. The depinning field can now be written as

$$H_d = -\frac{C_0(T)}{C_1(T)} - \frac{C_3(T)}{C_1(T)}j_d = b j_d^3 + c j_d^2 + d j_d + e, \quad \text{(A6)}$$

where the right equal sign corresponds to the experimentally found behavior. $C_0(T)/C_1(T)$ is even in j_d while $C_3(T)j_d/C_1(T)$ is odd in j_d. Equation (A6) has to be fulfilled for the even and the odd terms. This yields

$$-\frac{C_0(T)}{C_1(T)} = c j_d^2 + e \quad \text{(A7)}$$

for the even terms and

$$-\frac{C_3(T)}{C_1(T)} = b j_d^2 + d \quad \text{(A8)}$$

for the odd terms. From the last equation, one can calculate the spin-torque efficiency

$$\epsilon = \left|\frac{C_3(T)}{C_1(T)}\right| = \left|b j_d^2 + d\right|. \quad \text{(A9)}$$

Thus the symmetry consideration, i.e., leading to Eqs. (A7) and (A8), allows us to calculate the spin-torque efficiency for the experimental dependence between the depinning field and the depinning current.

Concerning Eq. (A6), one could argue that the experimental observation extends to the regime of $j_d > 0$ only and it is thus not clear whether $H_d = b j_d^3 + c j_d^2 + d j_d + e$ holds for negative values of j_d. However, Eqs. (A7) and (A8) can also be derived when we assume that the prefactors can be expanded in a power series of T. This assumption should be valid since we are far below the Curie temperature of the ferromagnet. Equation (A6) then reads

$$\begin{aligned}\sum_{k=0}^{\infty}\frac{d^k C_0}{dT^k}(T_0)\frac{a^k j_d^{2k}}{k!} + \sum_{k=0}^{\infty}\frac{d^k C_3}{dT^k}(T_0)\frac{a^k j_d^{2k+1}}{k!} \\ = -\sum_{k=0}^{\infty}\frac{d^k C_1}{dT^k}(T_0)\frac{a^k j_d^{2k+3}}{k!}b - \sum_{k=0}^{\infty}\frac{d^k C_1}{dT^k}(T_0)\frac{a^k j_d^{2k+2}}{k!}c \\ -\sum_{k=0}^{\infty}\frac{d^k C_1}{dT^k}(T_0)\frac{a^k j_d^{2k+1}}{k!}d - \sum_{k=0}^{\infty}\frac{d^k C_1}{dT^k}(T_0)\frac{a^k j_d^{2k}}{k!}e.\end{aligned} \quad \text{(A10)}$$

Equating the coefficients of even powers of j_d yields Eq. (A7), while equating the coefficients of odd powers of j_d yields Eq. (A8).

*bbeyersd@physnet.uni-hamburg.de

†Present address: Department of Physics, National Tsing Hua University, Hsinchu, Taiwan.

[1] S. S. P. Parkin, M. Hayashi, and L. Thomas, Science **320**, 190 (2008).

[2] R. P Cowburn, Nat. Mater. **6**, 255 (2007).

[3] A. Yamaguchi, T. Ono, S. Nasu, K. Miyake, K. Mibu, and T. Shinjo, Phys. Rev. Lett. **92**, 077205 (2004).

[4] G. Tatara and H. Kohno, Phys. Rev. Lett. **92**, 086601 (2004).

[5] J. Xiao, A. Zangwill, and M. D. Stiles, Phys. Rev. B **73**, 054428 (2006).

[6] A. Vanhaverbeke and M. Viret, Phys. Rev. B **75**, 024411 (2007).

[7] G. Tatara, H. Kohno, and J. Shibata, J. Phys. Soc. Jpn. **77**, 031003 (2008).

[8] M. Kläui, D. Ilgaz, L. Heyne, J. S. Kim, O. Boulle, C. Schieback, F. Zinser, S. Krzyk, M. Fonin, U. Rüdiger, D. Backes, L. J. Heyderman, T. O. Mentes, and A. Locatelli, J. Magn. **14**, 53 (2009).

[9]O. Boulle, G. Malinowski, and M. Kläui, Mater. Sci. Eng., R **72**, 159 (2011).
[10]X. Waintal and M. Viret, Europhys. Lett. **65**, 427 (2004).
[11]S. Zhang and Z. Li, Phys. Rev. Lett. **93**, 127204 (2004).
[12]A. Thiaville, Y. Nakatani, J. Miltat, and Y. Suzuki, Europhys. Lett. **69**, 990 (2005).
[13]K. Gilmore, I. Garate, A. H. MacDonald, and M. D. Stiles, Phys. Rev. B **84**, 224412 (2011).
[14]M. Kläui, J. Phys.: Condens. Matter **20**, 313001 (2008).
[15]R. Allenspach and P. Eib, Physics **3**, 91 (2010).
[16]L. Thomas, M. Hayashi, X. Jiang, R. Moriya, C. Rettner, and S. S. P. Parkin, Nature (London) **443**, 197 (2006).
[17]L. Bocklage, B. Krüger, T. Matsuyama, M. Bolte, U. Merkt, D. Pfannkuche, and G. Meier, Phys. Rev. Lett. **103**, 197204 (2009).
[18]G. Meier, M. Bolte, R. Eiselt, B. Krüger, D.-H. Kim, and P. Fischer, Phys. Rev. Lett. **98**, 187202 (2007).
[19]L. Heyne, J. Rhensius, D. Ilgaz, A. Bisig, U. Rüdiger, M. Kläui, L. Joly, F. Nolting, L. J. Heyderman, J. U. Thiele, and F. Kronast, Phys. Rev. Lett. **105**, 187203 (2010).
[20]E. Martinez, L. Lopez-Diaz, O. Alejos, and L. Torres, Phys. Rev. B **77**, 144417 (2008).
[21]S. Hankemeier, K. Sachse, Y. Stark, R. Frömter, and H. P. Oepen, Appl. Phys. Lett. **92**, 242503 (2008).
[22]T. R. McGuire and R. I. Potter, IEEE Trans. Magn. **4**, 1018 (1975).
[23]OOMMF, http://math.nist.gov/oommf
[24]R. Frömter, S. Hankemeier, H. P. Oepen, and J. Kirschner, Rev. Sci. Instrum. **82**, 033704 (2011).
[25]G.-W. Chern, H. Youk, and O. Tchernyshyov, J. Appl. Phys. **99**, 08Q505 (2006).
[26]S. Hankemeier, A. Kobs, R. Frömter, and H. P. Oepen, Phys. Rev. B **82**, 064414 (2010).
[27]L. K. Bogart and D. Atkinson, Appl. Phys. Lett. **94**, 042511 (2009).
[28]R. D. McMichael and M. J. Donahue, IEEE Trans. Magn. **33**, 4167 (1997).
[29]A. Himeno, T. Okuno, T. Ono, K. Mibu, S. Nasu, and T. Shinjo, J. Magn. Magn. Mater. **286**, 167 (2005).
[30]M. Dagras, M. Laufenberg, D. Bedau, L. Vila, G. Faini, C. A. F. Vaz, J. A. C. Bland, and U. Rüdiger, J. Phys. D **240**, 1247 (2007).
[31]P. Lendecke, R. Eiselt, G. Meier, and U. Merkt, J. Appl. Phys. **103**, 073909 (2008).
[32]G. S. D. Beach, M. Tsoi, and J. L. Erskine, J. Magn. Magn. Mater. **320**, 1272 (2008).
[33]L. Thomas and S. S. P. Parkin, in *Handbook of Magnetism and Advanced Magnetic Materials* (Wiley, New York, 2007), Vol. 2.
[34]L. Bocklage, B. Krüger, R. Eiselt, M. Bolte, P. Fischer, and G. Meier, Phys. Rev. B **78**, 180405 (2008).
[35]D. Bedau, M. Kläui, U. Rüdiger, C. A. F. Vaz, J. A. C. Bland, G. Faini, L. Vila, and W. Wernsdorfer, J. Appl. Phys. **101**, 09F509 (2007).
[36]T. Kimura, Y. Otani, K. Tsukagoshi, and Y. Aoyagi, J. Appl. Phys. **94**, 7947 (2003).
[37]S. Lepadatu, A. P. Mihai, J. S. Claydon, F. Maccherozzi, S. S. Dhesi, C. J. Kinane, S. Langridge, and C. H. Marrows, J. Phys.: Condens. Matter **24**, 024210 (2012).
[38]M. Laufenberg, W. Bührer, D. Bedau, P.-E. Melchy, M. Kläui, L. Vila, G. Faini, C. A. F. Vaz, J. A. C. Bland, and U. Rüdiger, Phys. Rev. Lett. **97**, 046602 (2006).
[39]M. C. Hickey, D.-T. Ngo, S. Lepadatu, D. Atkinson, D. McGrouther, S. McVitie, and C. H. Marrows, Appl. Phys. Lett. **97**, 202505 (2010).
[40]M. Hayashi, L. Thomas, C. Rettner, R. Moriya, and S. S. P. Parkin, Appl. Phys. Lett. **92**, 162503 (2008).
[41]S. Lepadatu, M. C. Hickey, A. Potenza, H. Marchetto, T. R. Charlton, S. Langridge, S. S. Dhesi, and C. H. Marrows, Phys. Rev. B **79**, 094402 (2009).
[42]This is the more probable as the same authors find just the opposite temperature dependence of critical current densities for a different sample.[30] In fact, the current-dependent critical field graphs published there show constant slopes, independent of substrate temperature, so from the cited data, an extension of our observation of constant epsilon down to liquid helium temperatures could be concluded.
[43]G. Tatara, T. Takayama, H. Kohno, J. Shibata, Y. Nakatani, and H. Fukuyama, J. Phys. Soc. Jpn. **75**, 064708 (2006).
[44]M. Zhu, C. L. Dennis, and R. D. McMichael, Phys. Rev. B **81**, 140407 (2010).